IC Engine Power Maximized at Recommended Operating Conditions

AUTHOR
PARTH PATEL

RECIPIENT
WEBB INDUSTRIES
ATTN: JULIE CHANG

DATE
APRIL 3rd, 2026

CLASS & SECTION
ME 3058, L05

SUPERVISORS
DAVID MACNAIR
CHASE SUN
JILL FENNELL

- IMRAN AZIZ
- LUKE GRIFFIN

BURDELL, INC.
ANALYTICAL DIVISION

Introduction

Webb Industries is developing a modular generator that utilizes compressed air rather than combustible fuel to drive an electric motor and store excess energy in an attached battery pack. To ensure the commercial viability of this system, predictive models must accurately account for real world physical losses. This report presents an experimental energy balance analysis of a pneumatic internal combustion engine system for Webb Industries, characterizing friction, flywheel inertia, and air work to optimize power output. The friction model was determined as $T_f(\omega) = 0.00807\omega + 0.494$ Nm, flywheel inertia matched theoretical predictions within 3.1 percent, and experimental air work reached only 27 to 33 percent of adiabatic predictions due to cylinder leakage and heat transfer losses. Based on these findings, the primary recommendation is that operating the engine at a 0.8 volts motor setting with an air injection window of 310 degrees to 20 degrees relative to top dead center produces the maximum reliable power output of 97.9 Watts per cycle. We recommend adopting these specific parameters because they perfectly balance the time dependent air leakage at low speeds against the speed dependent mechanical drag at high speeds.

Methodology

The methodology for this experiment was structured so that each unknown component of the engine energy balance could be determined sequentially. Torque measurements were first calibrated to ensure accurate force measurements. Friction was then characterized so that the friction work could be separated from total system work. The flywheel moment of inertia was determined using transient energy methods. With friction and inertia known, the system energy balance was used to determine the work of air. Engine power was then calculated, and air intake timing was optimized to maximize power output. Uncertainty analysis was performed throughout the calculations to quantify measurement error and confidence in the results.

Torque Sensor Calibration

Before engine testing began, the force transducer used to measure torque was calibrated to convert measured voltage signals into torque values. Known calibration weights with predetermined masses were applied to the torque arm at a known moment arm length, allowing the applied torque for each test point to be calculated using the relationship

$$T = r \cdot W \tag{1}$$

where the weight force was determined from the mass of the calibration weights. Multiple weights and combinations of weights were used to generate several calibration points over the expected operating range of the transducer. Both loading and unloading measurements were recorded to account for hysteresis effects in the sensor and to ensure the calibration captured any differences in sensor response during increasing and decreasing loads.

The measured force transducer voltage was recorded for each applied torque value, and a linear regression was performed to determine the relationship between voltage and torque. The calibration data and regression line are shown in Figure 1 as an example of the calibration relationship used.

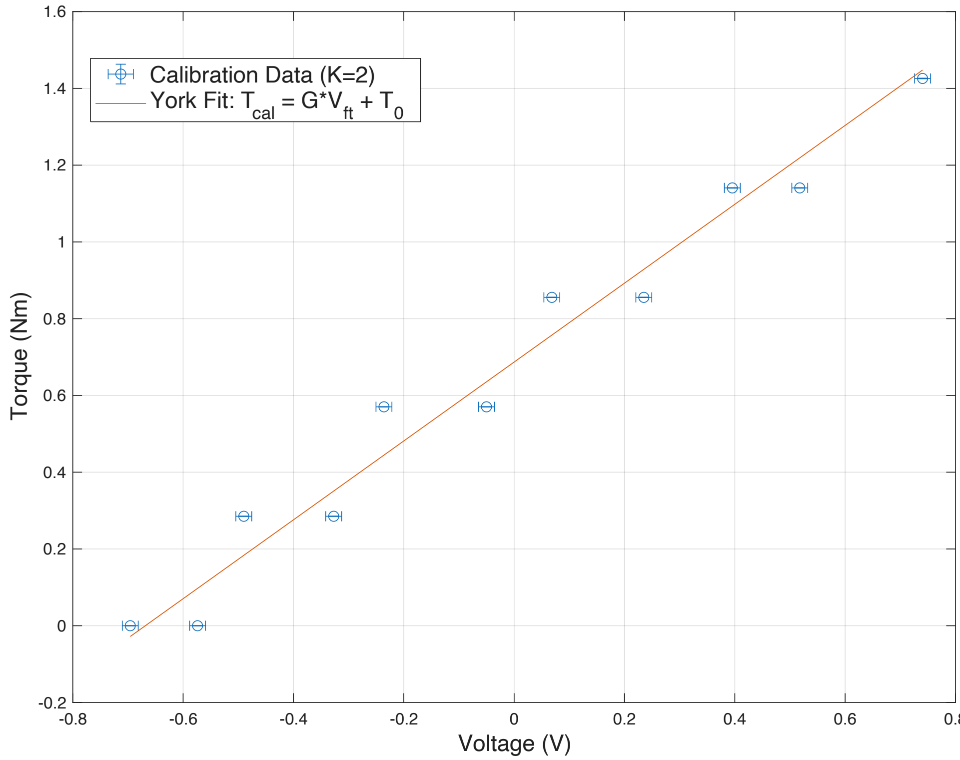

Figure 1: Calibration plot to relate sensor voltage to the corresponding torque and develop an equation to use for use in calculating motor torque

The resulting linear calibration equation was then used to convert all measured voltage signals during engine testing into torque values using

$$T_{cal} = G \cdot V_{ft} + T_0 \tag{2}$$

where $G$is the calibration gain and $T_0$is the torque offset. This calibration procedure was necessary because all work and power calculations throughout the engine cycle were based directly on torque measurements, so accurate conversion from voltage to torque was required before any engine performance analysis could be performed.

Friction Characterization

To characterize frictional losses in the system, the engine was operated without the engine head so that no compression or air work occurred. Under these conditions, the only torques acting on the system were motor torque and friction torque. At steady state, the angular velocity of the flywheel is constant, meaning there is no change in flywheel energy and motor torque balances friction torque. Friction torque was measured at multiple engine speeds and modeled as a linear combination of Newtonian and Coulomb friction models, in the form

$$T_{friction} = a \cdot RPM + b \tag{3}$$

This friction model was later used to calculate friction work and isolate the work contributions from other components of the system.

Flywheel Moment of Inertia Determination

The flywheel moment of inertia was determined by analyzing the transient acceleration of the engine from rest to steady state. During acceleration, the change in flywheel kinetic energy is equal to the net work done on the system after accounting for friction losses. The flywheel energy was calculated using

$$E_{fly} = \frac{1}{2} I_{fly} \omega^2 \tag{4}$$

By measuring angular velocity during acceleration and accounting for motor work and friction work, the moment of inertia for different flywheel configurations was calculated. Multiple flywheel configurations were tested so that the inertia of a single flywheel could be determined from differences between configurations.

System Energy Balance and Work Calculations

Once friction and flywheel inertia were characterized, the engine was operated with the engine head installed and compressed air supplied to the intake. The system energy balance was used to account for all work contributions in the engine cycle, including motor work, friction work, piston work, and work of air. The governing energy balance for the system was

$$E_{fly,b} - E_{fly,a} = -W_{motor} + W_{friction} + W_{piston} + W_{air} + W_{error} \tag{5}$$

Torque data was collected over multiple engine cycles and integrated over angular displacement to determine work done during each portion of the engine cycle. This energy balance allowed the work of air to be isolated by subtracting known work contributions from the total work acting on the flywheel.

Work of Air Analysis

The work done by air during compression and expansion strokes was determined experimentally from torque integration and compared to theoretical work values calculated using compressible gas relations assuming adiabatic compression and expansion. The theoretical work of air between two states was calculated using

$$w_{air,a\to b} = \frac{P_a V_a^{\gamma}}{1-\gamma}\left(V_b^{1-\gamma} - V_a^{1-\gamma}\right) - P_{atm}(V_b - V_a) \tag{6}$$

This model assumed ideal gas behavior, no leakage, and negligible heat transfer. Comparing experimental and theoretical work values allowed non-ideal effects such as leakage, heat transfer, and flow restrictions to be evaluated.

Power Calculation and Operating Conditions

Engine power output was determined from torque and engine speed measurements. The electric motor driving the crankshaft was operated at various voltages to change engine speed, and torque data was collected at steady-state operation. Power output was calculated using

$$Power = Torque \cdot RPM \tag{7}$$

This analysis allowed identification of operating conditions where compressed air contributed the greatest positive work to the system and established the baseline operating condition used for intake timing optimization.

Air Intake Timing Optimization

The final portion of the experiment focused on maximizing engine power by optimizing the air intake opening angle and intake duration relative to piston position. Intake opening angle was varied relative to top dead center while holding intake duration constant to determine the optimal opening angle. After determining the optimal opening angle, intake duration was varied to determine the optimal window size. Power output was calculated by integrating steady-state torque over engine rotation using

$$W_{motor} = \sum T_{motor} \Delta\theta \tag{8}$$

This optimization procedure allowed identification of the intake timing parameters that produced the maximum engine power output.

Results

Friction analysis reveals a combined Coulomb and Newtonian model, $T_f(\omega) = 0.00807\omega + 0.494\ Nm$ (R^2 = 0.9352), sufficient for downstream work calculations despite minor nonlinear residuals. Flywheel inertia scales linearly with flywheel count (R^2 = 0.9985), with an experimental per-flywheel inertia of 0.002594 kg·m² deviating only 3.1% from the theoretical value of 0.002677 kg·m². Work of air analysis confirms the engine behaves as a conservative energy exchanger without combustion, producing near-zero net cycle work (-0.58 J to +1.00 J), with experimental compression and power work reaching only 27-33% of theoretical adiabatic predictions due to cylinder leakage and heat transfer losses. With pneumatic air injection, net positive work output is achievable, with an optimal injection window of 310° to 20° at 0.8 V producing a maximum of 97.9 W per cycle.

Combined Newtonian and Coulomb Friction Model

Frictional torque in the IC engineer flywheel system increases with angular velocity, indicating a combined Coulomb and Newtonian friction model rather than either idealized model alone. At steady state, zero net acceleration means motor torque directly equals friction torque. This allows steady-state motor torque measurements across five voltage settings to serve as friction torque observations at known speeds. Measured friction torque ranged from 0.6374 Nm at 21.68 rad/s to 0.9989 Nm at 68.05 rad/s, confirming a speed-depended relationship. As shown in Figure 2, a linear regression of five data points across five different input voltages yields the friction model, $T_f(\omega) = 0.00807\omega + 0.494\ Nm$.

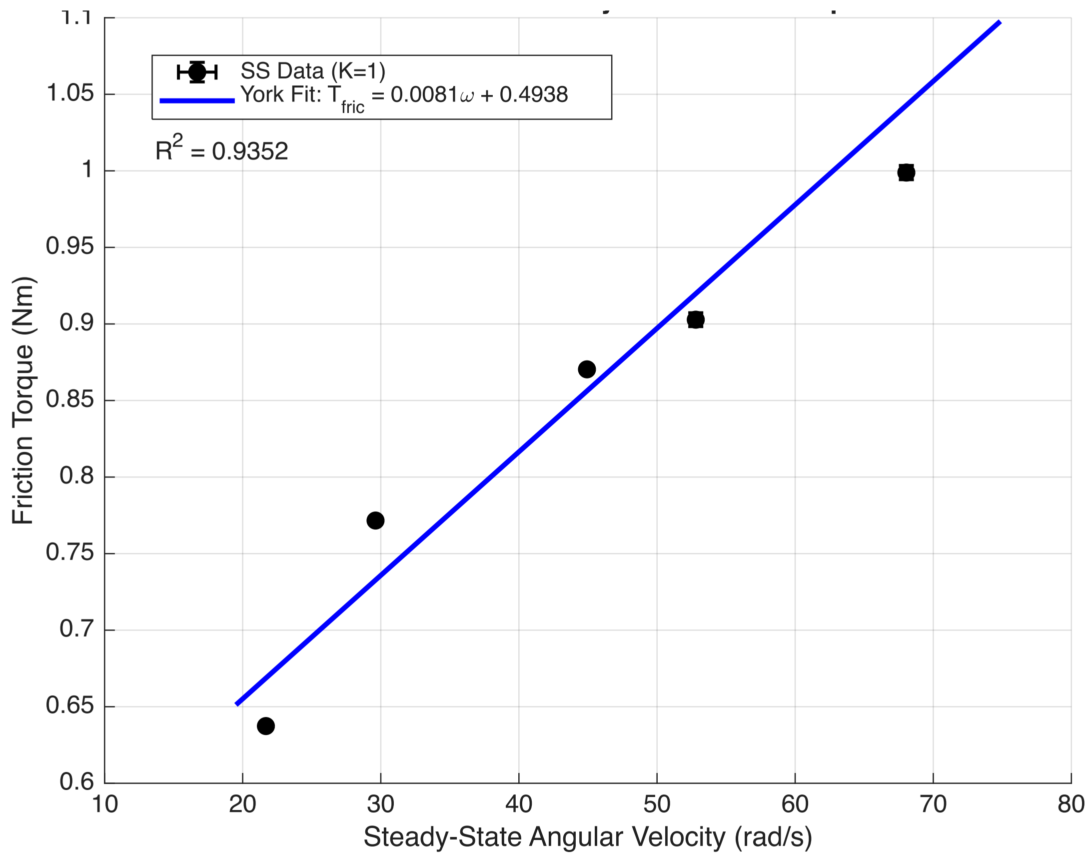

Figure 2: Angular velocity vs. Friction torque with a York fit line to show the friction model equation

The non-zero slope of $0.00807 \pm 0.000175\ \frac{Nm}{rad/_s}$ quantifies the Newtonian component where torque increases proportionally with speed. The y-intercept of $0.494 \pm 0.00659\ Nm$ represents the speed-independent Coulomb component that persists even as the engine approaches rest.

The R^2 of 0.9352 confirms that the linear combined model captures the dominant friction behavior across the operating range, the remaining 6.5% of unexplained variance suggests minor nonlinear friction effects such as static friction or bearing drag that the two-term model does not fully resolve. However, the calibration uncertainty of $\pm 0.00595\frac{Nm}{V}$ on the force transducer gain propagates into each torque measurement, meaning a portion of this residual variance is attributable to measurement noise rather than true model deficiency. Given that the model uncertainty bounds ($\pm 0.000175\ \frac{Nm}{rad/_s}$ and $\pm 0.00659\ Nm$) remain small relative to the measured torque range of 0.6374 to 0.9989 Nm, the linear combined model is sufficiently precise for computing friction work.

Flywheel Inertia Matches Theoretical Predictions

Experimental flywheel inertia scales linearly with flywheel count and agrees with the theoretical value to within 3.1%, validating the measurement method. A linear regression of mean inertias across all five flywheel configurations (0 to 4) isolates the per-flywheel contribution by treating the unknown shaft inertia as a constant offset, yielding $I_{base} = 0.001131\ kg \cdot m^2$ and $I_{per\ fly} = 0.002594\ kg \cdot m^2$, as shown in Figure 3. The R^2 of 0.9985 confirms that inertia scales linearly with flywheel count across all five configurations, and the experimental $I_{per\ fly}$ value deviates from $I_{theoretical} = 0.002677\ kg \cdot m^2$ by only 3.1%, confirming that the theoretical model accurately represents the physical system.

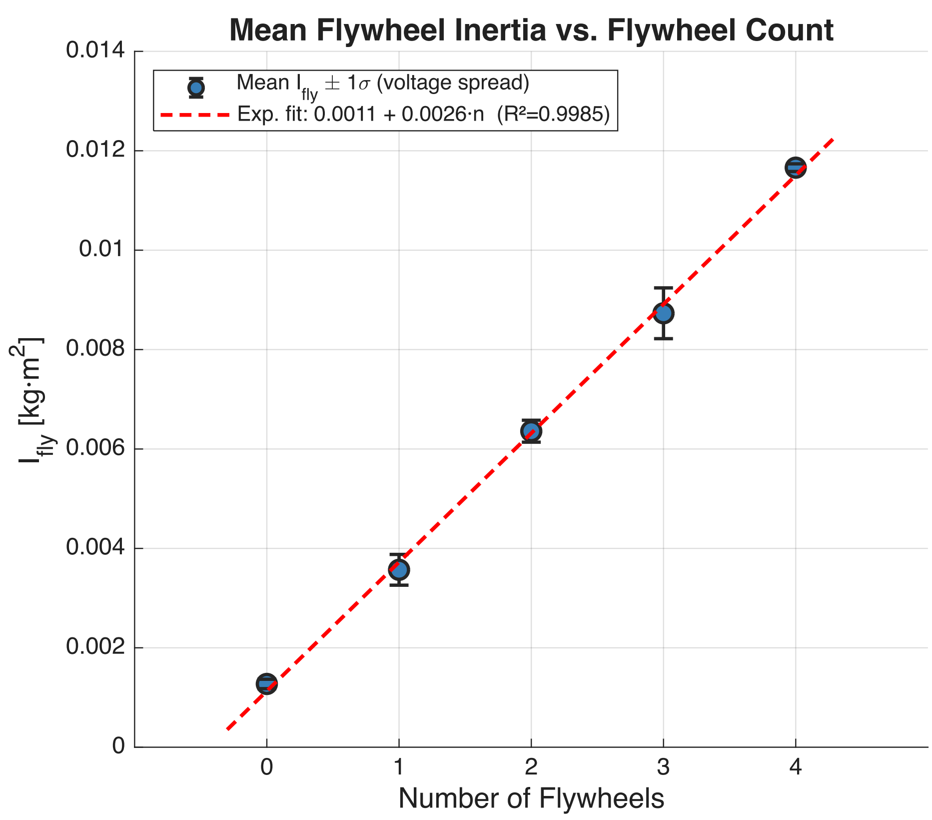

Figure 3: Mean flywheel inertia vs flywheel count with regression fit line

Moment of inertia measurements vary systematically with motor voltage setting across all flywheel configurations, with 6V consistently producing the highest inertia values and 3V and 9V bracketing lower, as shown in Table 1. This pattern is too consistent across all five configurations to be attributable to random measurement noise and is instead traceable to nonlinearity in the friction model. As established in the friction model section, the friction model linear fit carries an R^2 of 0.9352, meaning the model foes not perfectly capture friction torque at all operating speeds. At 3V and 9V, the friction model overestimates friction torque, causing friction work to be over-subtracted from motor work in the energy balance, which suppresses the calculated inertia value. At 6V, the inverse occurs: friction torque is underestimated, inflating the calculated inertia value.

Table 1: Moment of inertia for five flywheel configurations

Config	3V (kgm^2)	6V (kgm^2)	9V (kgm^2)	Mean
0 fly	0.001312	0.001341	0.001165	0.001273
1 fly	0.003393	0.003927	0.003389	0.003569
2 fly	0.006285	0.006606	0.006183	0.006358
3 fly	0.008352	0.009312	0.008527	0.00873
4 fly	0.011587	0.01174	0.011652	0.01166

Despite this RPM-depended bias, the mean inertia values across voltage settings converge tightly for each flywheel configuration, with uncertainties ranging from 0.0something to 0.0something supporting the use of mean inertia values in the linear regression and downstream analysis.

Torque Cycle and Work of Air

Numerical integration of the representative averaged torque cycles across all four strokes reveals that the IC engine operating on compressed air performs near-zero net work per cycle, confirming that the system behaves as a conservative exchanger rather than a net power producer in the absence of combustion. Across all tested configurations, compression produces negative air work as the piston compresses the cylinder charge, and the power stroke recovers positive work as the expanding air drives the piston downward. This cycle is also exemplified by the torque and velocity cycles as shown in Figure 4.

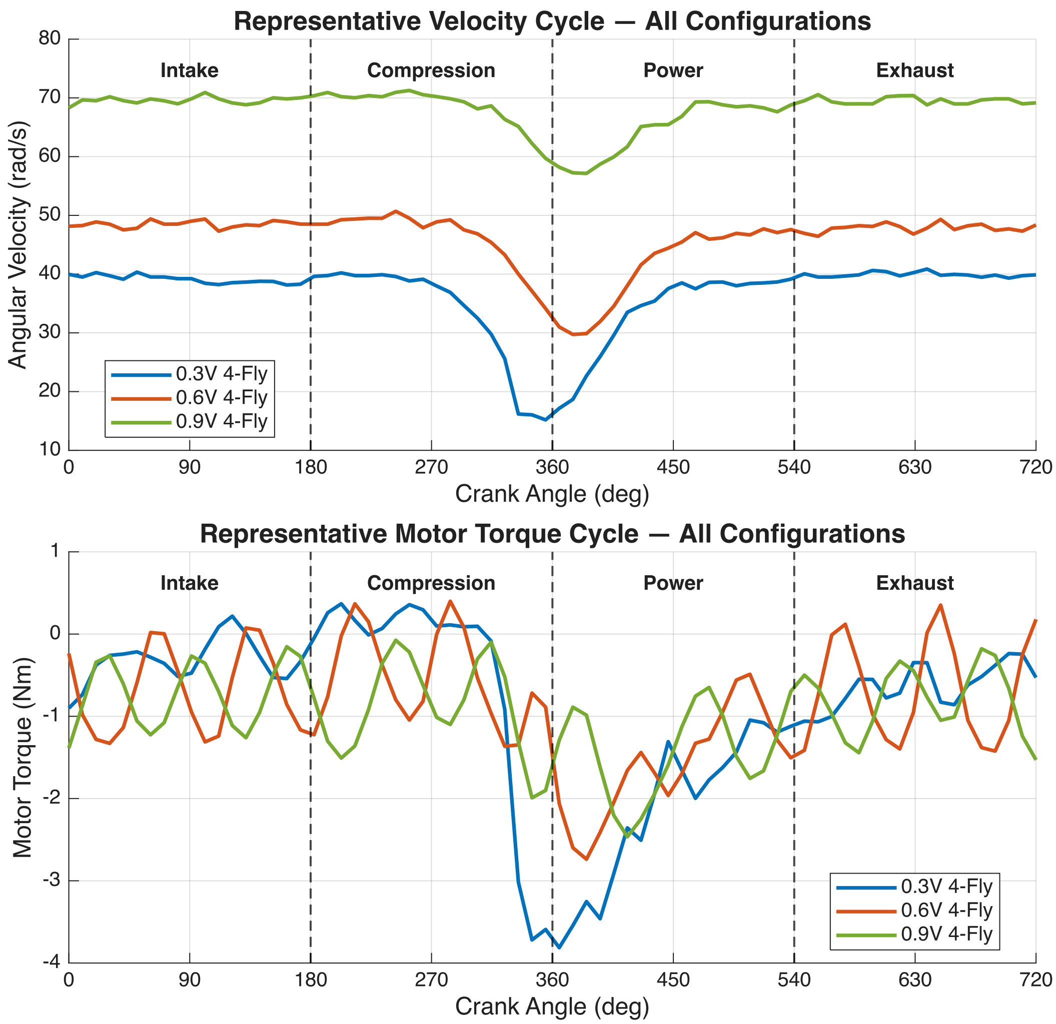

Figure 4: Velocity and Torque over four stroke cycle for 0.3, 0.6, and 0.9V with 4-fly configurations

The net work per cycle (sum across all four strokes) ranges from -0.58J to +1.00J as shown in Table 2. The near-zero net values confirm that energy stored during compression is substantially recovered during expansion, consistent with a system operating without a combustion event to add net energy to the cycle. The non-zero intake and exhaust work values of 0.78 – 2.21J and 0.43 – 1.36J respectively, which theoretically should be zero for ideal open strokes, indicated real valve timing imperfections and gas exchange inefficiencies in the physical engine.

Table 2: Net work summary table across all four strokes and four different testing configurations

Config	**Intake (J)**	**Compression (J)**	**Power (J)**	**Exhaust (J)**	**Net (J)**
1-fly 6V	$+1.66 \pm 0.0064$	-6.94 ± 0.79	$+3.54 \pm 0.91$	$+1.16 \pm 0.14$	-0.58
1-fly 9V	$+1.82 \pm 0.033$	-7.75 ± 0.95	$+5.14 \pm 1.08$	$+1.36 \pm 0.12$	$+0.57$
4-fly 6V	$+0.78 \pm 0.036$	-6.43 ± 0.28	$+4.36 \pm 0.25$	$+1.23 \pm 0.049$	-0.06
4-fly 9V	$+2.21 \pm 0.056$	-7.89 ± 0.32	$+6.25 \pm 0.28$	$+0.43 \pm 0.035$	$+1.00$

Work of air magnitude during compression and power strokes increases consistently with motor voltage across both flywheel configurations, and experimental values deviate substantially from the theoretical adiabatic model across all tested conditions. At 6V, the 4-flywheel configuration produces compression and power work of -6.43 J and +4.36 J respectively, increasing to -7.89 J and +6.25 J at 9V, with the same trend holding for the 1-flywheel configuration, as shown in Table X. At higher RPM, each stroke is completed in less time, reducing heat transfer through cylinder walls and air leakage past piston rings, pushing the process incrementally closer to adiabatic behavior.

Despite this trend, experimental compression and power work magnitudes reach only 27-33% of the theoretical ±23.41 J across all configurations and speeds, with discrepancies ranging from 15.66 J to 20.13 J, all well outside experimental uncertainty bounds. The consistency of this discrepancy across configurations and RPM settings confirms it reflects a real physical limitation of the adiabatic model rather than measurement error. The adiabatic model assumes a perfectly sealed, lossless cylinder, but the physical engine loses significant energy to piston ring leakage and heat transfer. These losses reduce the effective compression ratio and recoverable expansion work by approximately a factor of three, proving that a polytropic model accounting for leakage would be required to accurately predict air work in this system.

Optimal Intake Timing Maximizes Power Output

Maximum mechanical power output is achieved when the pneumatic injection window is timed to balance maximum expansion volume against upward stroke resistance, with an optimal configuration of 310° to 20° at 0.8 V producing a peak output of 97.9 W. Power output depends on net work per cycle and engine speed per Equation 6, where compressed air introduced into the cylinder overcomes baseline frictional and inertial losses to yield net positive power generation. The magnitude of generated power is highly sensitive to injection window timing, initiating injection before top dead center allows pneumatic pressure to fully develop in the cylinder head as the piston begins its downward power stroke, maximizing the work extracted per Equation 5. A preliminary sweep of injection windows across 0.7, 0.8, and 0.9 V motor settings established this relationship, as shown in Figure 5. Peak power values of 105.4 W, 80.2 W, and 101.4 W were observed at 0.7, 0.8, and 0.9 V respectively across the wide window sweep, but the high variability across voltage settings necessitated a refined sweep over narrower injection windows to identify true optimal conditions.

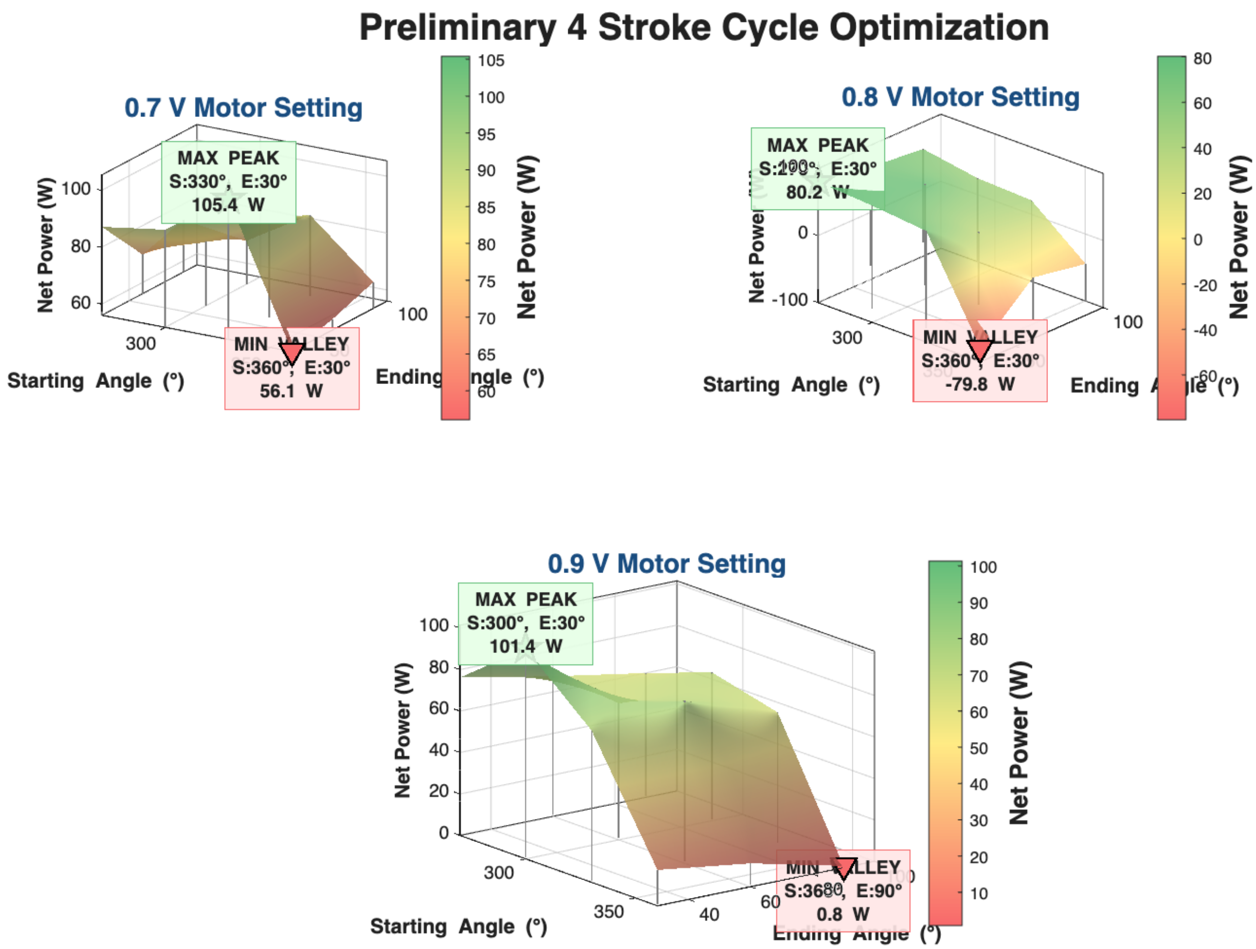

Figure 5: Preliminary contour maps of net engine power (W) at varying wide injection windows across 0.7, 0.8, and 0.9 volts motor settings

Refined testing over narrower injection windows confirms that 0.8 V produces the most consistent peak power output, balancing competing effects of air leakage and frictional drag that dominate at lower and higher speeds respectively, as shown in Figure 6. Injecting too early forces the flywheel to expend stored kinetic energy pushing the piston upward against incoming high-pressure air, reducing net power, while terminating injection too late wastes pressurized air at the bottom of the stroke. At 0.7 V, reduced engine speed allows more air to escape past the piston seals before conversion to shaft rotation, yielding a slightly reduced peak of 96.0 W. At 0.9 V, increased Newtonian frictional drag outpaces the pneumatic energy gained despite reduced leakage, dropping peak power to 89.0 W. The 0.8 V setting with a 310° to 20° injection window therefore represents the optimal balance between leakage losses and friction losses, producing the highest reliable power output of 97.9 W.

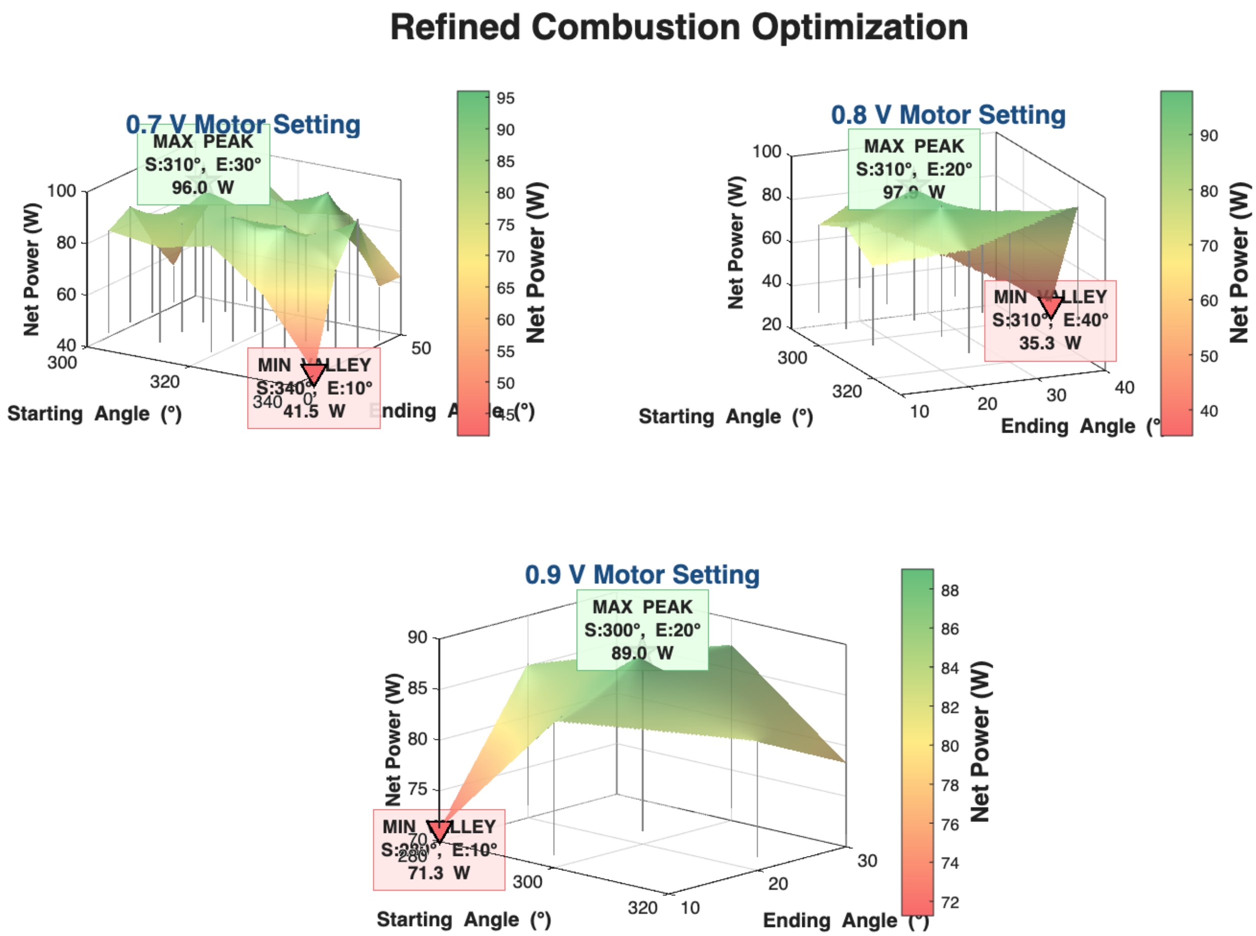

Figure 6: Refined contour maps of net engine power (W) at varying narrow injection windows across 0.7, 0.8, and 0.9 volts motor settings.

Conclusion

This experiment successfully characterized the internal combustion engine energy balance and identified optimal operating conditions for maximum pneumatic power output. The combined friction model and flywheel inertia measurements were validated against theoretical values, while work of air analysis revealed that leakage and heat transfer reduce effective air work to roughly one third of adiabatic predictions. This finding proves that a polytropic model would better represent this system in future analyses. Intake timing optimization identified an injection window of 310 degrees to 20 degrees at a 0.8 volts motor setting as the optimal configuration. This yields a peak output of 97.9 Watts by balancing air leakage losses at low speeds against Newtonian frictional drag at high speeds. Webb Industries is advised to adopt these parameters as the baseline operating condition for further development of this engine platform. Moving forward, utilizing this precisely tuned injection window ensures that the generator maximizes energy transfer to the battery pack without risking mechanical stalling. By updating their predictive software to incorporate the newly quantified thermal and fluid inefficiencies, the engineering team can confidently scale the generator design and accurately forecast overall power yields for future commercial deployment.